SOME PERFORMANCE IMPROVEMENTS TECHNIQUES

(148)

NONREDUNDANT ERROR CORRECTION RECEIVERS

- NEC is an attractive coding technique which has no rate redundancy.
- Coding at the receiver.
- Application to CCI channels.

Ref.

IEEE TRANSACTIONS ON VEHICULAR TECHNOLOGY, VOL. 41, NO. 1, FEBRUARY 1992

CUSTOMER COPY

Nonredundant Error Correction Analysis and Evaluation of Differentially Detected $\pi/4$–Shift DQPSK Systems in a Combined CCI and AWGN Environment

Dominic P. C. Wong and P. Takis Mathiopoulos, *Member, IEEE*

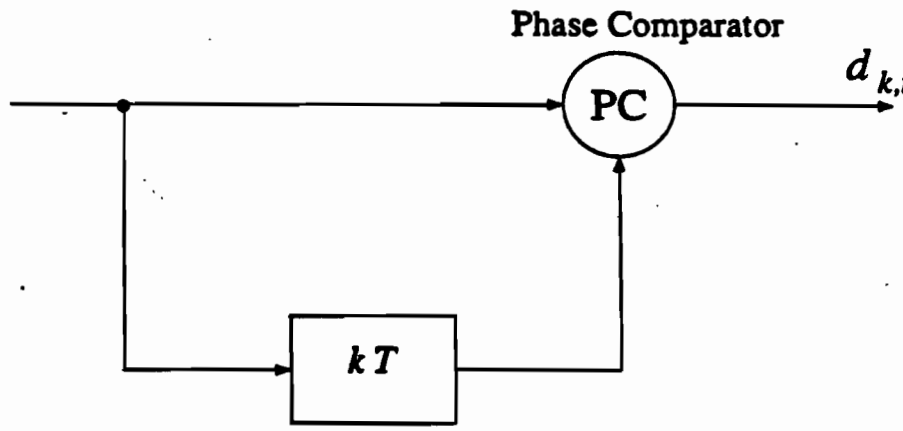

Figure 2 A k-th order differential detector

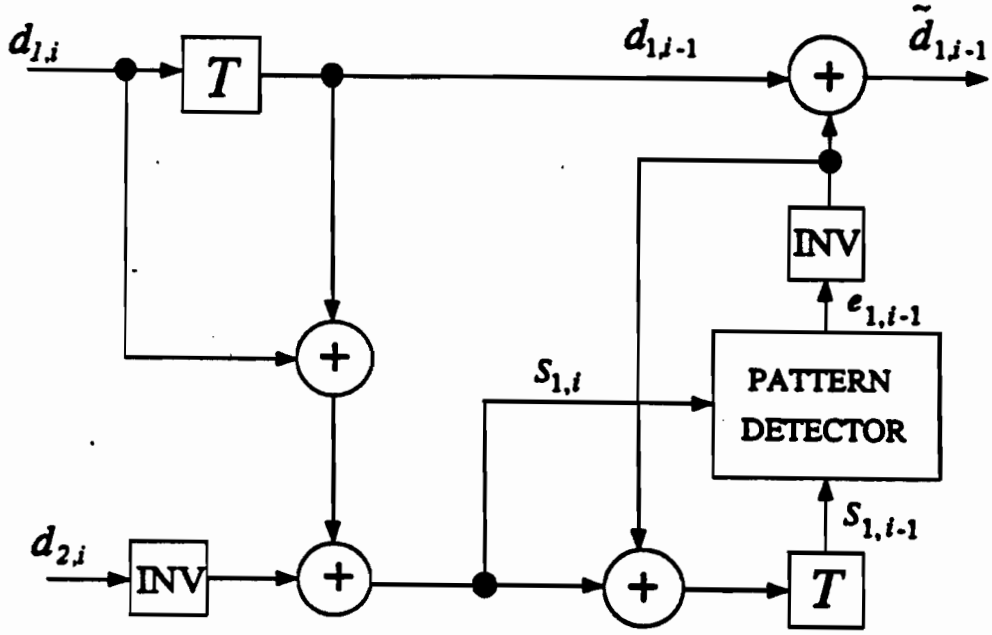

Figure 3 Block diagram of the single error correction NEC receiver for a $\pi/4$-shift DQPSK system. All inverters (INV) and adders are of mod-8.

Table 3 Relationship between the syndromes $S_{1,i}$, $S_{1,i-1}$ and the error $e_{1,i-1}$. $n \in \{1, 3\}$

$S_{1,i}$	$S_{1,i-1}$	$e_{1,i-1}$
0	0	0
0	$n \neq 0$	0
$n \neq 0$	0	0
$n \neq 0$	$n \neq 0$	$n \neq 0$

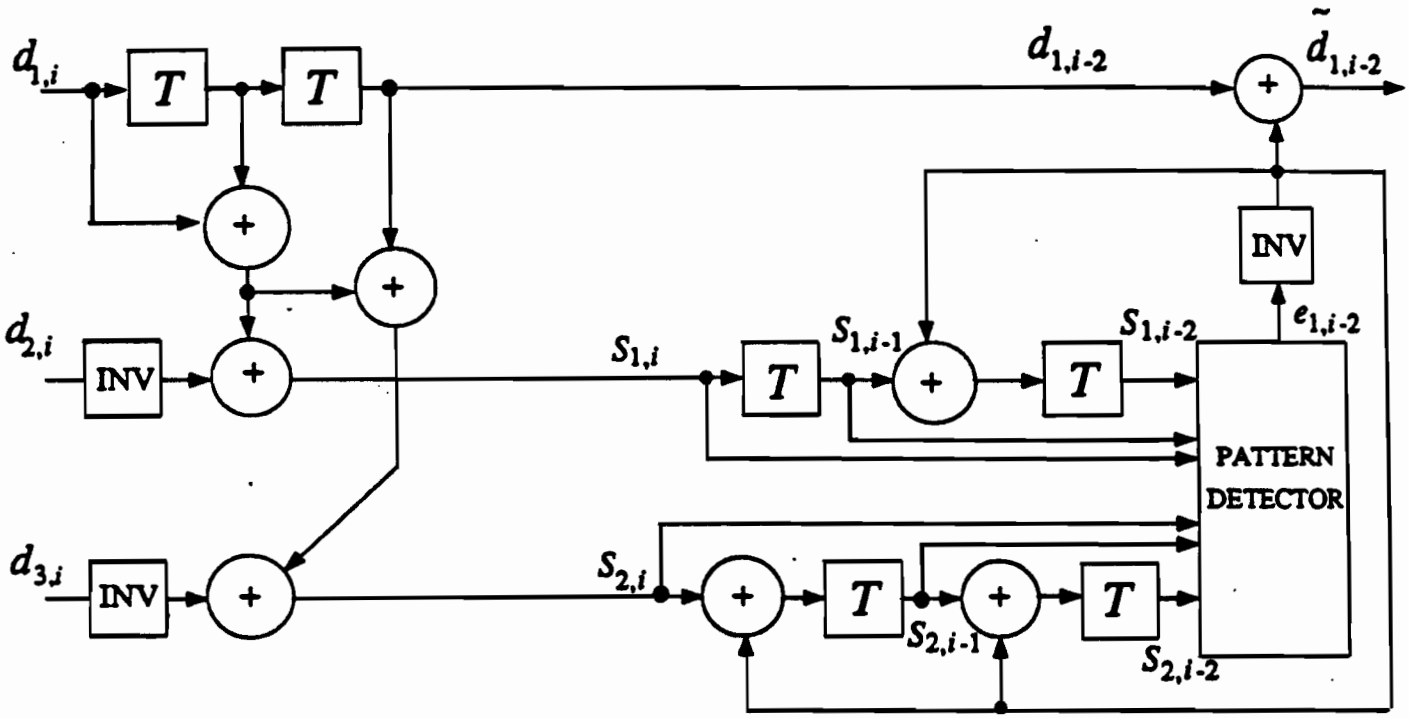

Figure 4 Block diagram of the double error correction NEC receiver for a $\pi/4$-shift DQPSK system. All inverters (INV) and adders are of mod-8.

Table 4 Detection patterns for the error symbol $e_{1,i-2}$ of the second order NEC (see also Fig. 4). $n \in \{1,3\}$, $m \in \{0,1,3\}$.

$S_{1,i}$	$S_{1,i-1}$	$S_{1,i-2}$	$S_{2,i}$	$S_{2,i-1}$	$S_{2,i-2}$	$e_{1,i-2}$
m	n	n	$m+n$	n	n	n
m	$m+n$	n	$m+n$	$m+n$	n	n
m	n	n	n	n	n	n
0	$n-m$	n	n	n	n	n
0	n	$n-m$	n	n	n	n
0	n	n	$n-m$	n	n	n
0	n	n	n	$n-m$	n	n
0	n	n	n	n	$n-m$	n

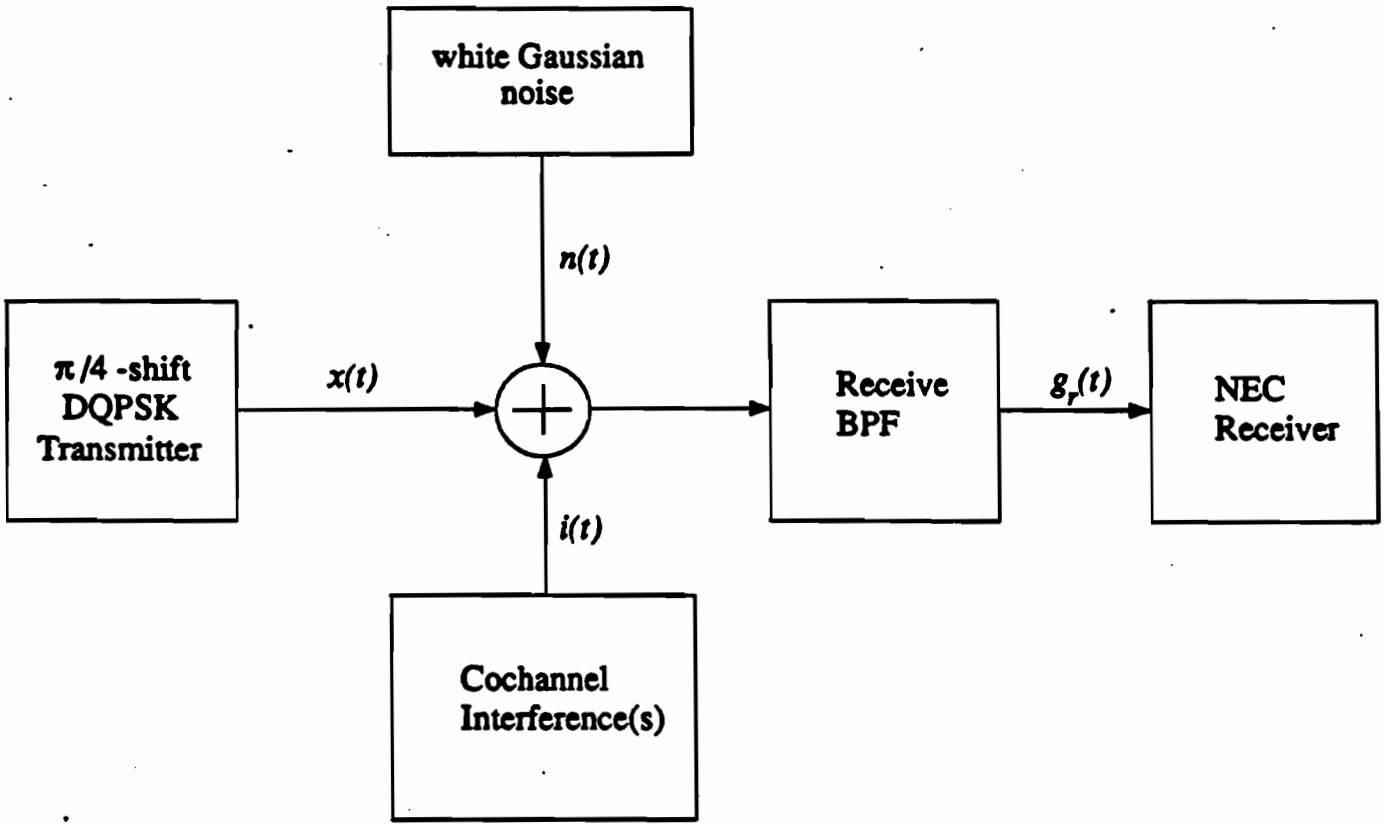

Figure 6 The general block diagram of the digital communication system under consideration.

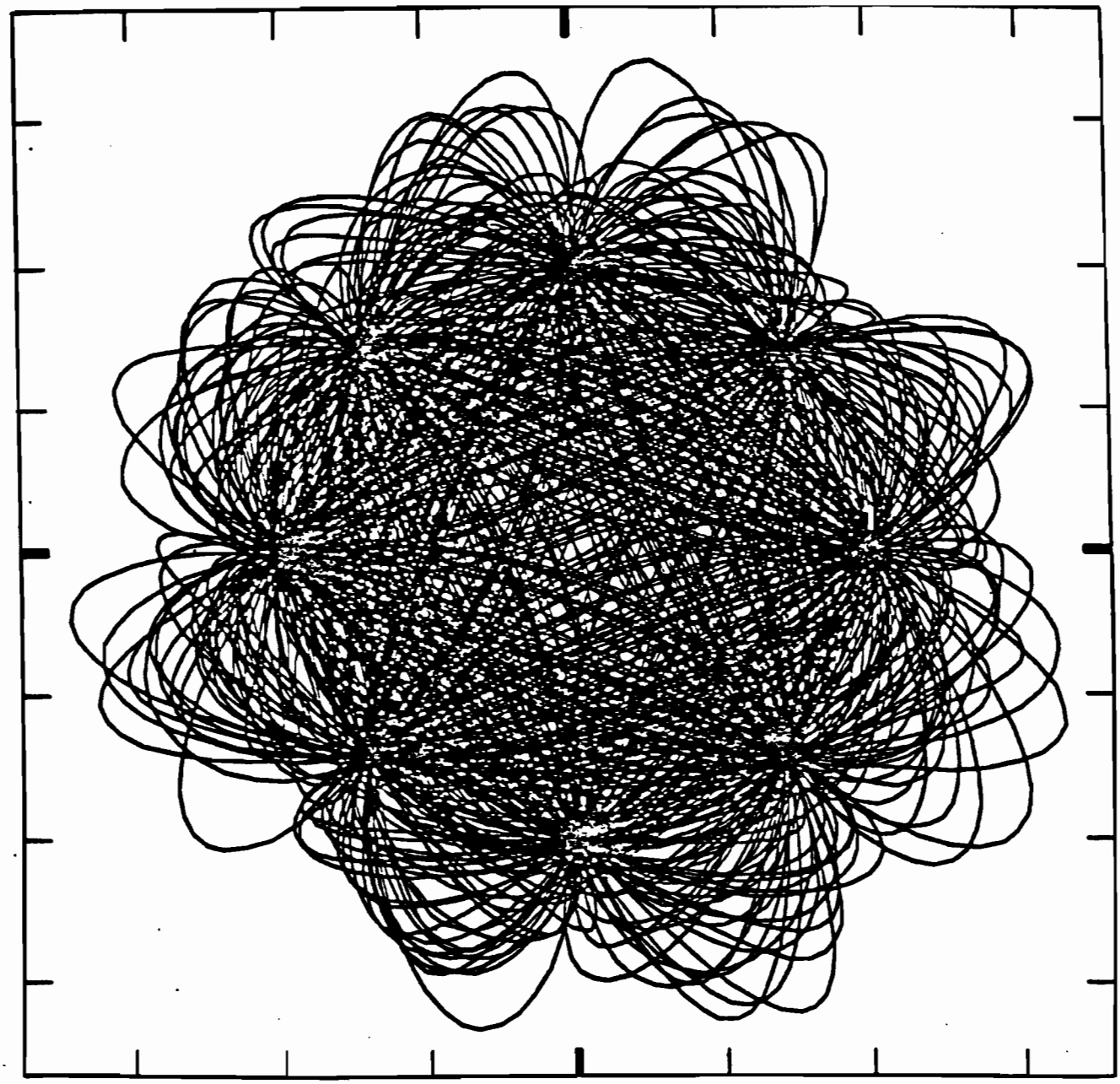

Figure 9 State-space diagram of a computer-simulated $\pi/4$–shift DQPSK system employing raised cosine filters with an excess bandwidth of 35% and which is operated in the presence of CCI (C/I= 55 dB) and Gaussian noise (C/N=60 dB). The number of interferers is equal to 4.

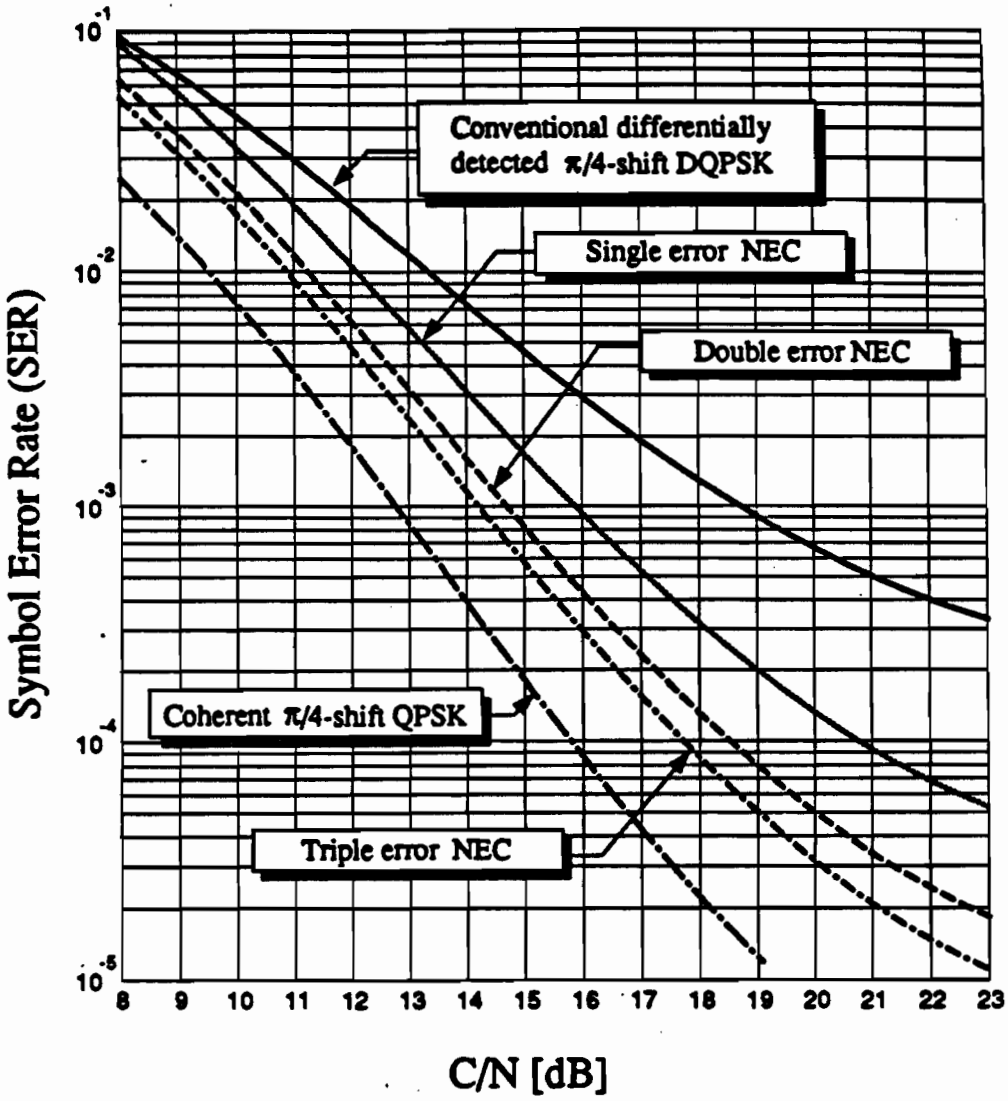

Figure 11 Symbol error rate performance of the NEC with infinitive interferers at C/I=14 dB.

Table 10 Theoretical performance gains of a differentially detected $\pi/4$–shift DQPSK system employing various NEC receivers and operated in a CCI environment. All gains reported are with reference to a conventional differentially detected $\pi/4$–shift DQPSK system. Although here *error floor* refers to the performance of a conventional differentially detected $\pi/4$–shift DQPSK system, it is clear from the obtained performance evaluation results that the NEC system reduces these error floors.

		C/N Gain at SER = 10^{-2} [dB]			C/N Gain at SER = 10^{-4} [dB]		
C/I [dB]	*M*	Single-Error NEC Receiver	Double-Error NEC Receiver	Triple-Error NEC Receiver	Single-Error NEC Receiver	Double-Error NEC Receiver	Triple-Error NEC Receiver
10	1	2.0	3.8	4.7	3.0	4.5	5.8
	6	*error floor*	*error floor*	*error floor*	*error floor*	*error floor*	*error floor*
	∞	*error floor*	*error floor*	*error floor*	*error floor*	*error floor*	*error floor*
14	1	1.1	2.0	2.3	1.6	2.6	3.1
	6	1.2	2.1	2.5	5.0	6.8	7.4
	∞	1.3	2.2	2.5	*error floor*	*error floor*	*error floor*
18	1	0.8	1.5	1.8	1.3	2.0	2.3
	6	0.8	1.5	1.8	1.6	2.2	2.6
	∞	0.8	1.5	1.8	1.6	2.3	2.7

THE "BEST" RECEIVER FOR THE FADING CHANNEL

We were the first to theoretically derive the optimal noncoherent receiver for the fading channel. Optimal refers to the receiver which results in the "best" achievable performance.

Our derivation is very general and it includes:

- Any signals (PSK or QAM)
- No assumption about the fading (e.g., that it stays constant over the symbol duration).
- Any fading model.
- No carrier recovery is required → no decoding delays.
- No redundancy (e.g., pilot tones in the time or frequency).

Ref. Optimal decoding of coded PSK and QAM signals in correlated fast fading channels and AWGN : A combined envelope, multiple differential and coherent detection approach.

by D. MAKRAKIS, P. T. MATHIOPOULOS, D. P. BOURAS

IEEE Trans. Commun. Jan. 1994 (pp. 63-75)

COMMENTS

1. The proposed receivers are the equvilent of the "Viterbi Decoders" for the AWGN channel.
2. Performance gains with minimal complexity.
3. Very generic structure and therefore could be used for both current and future wireless personal communication systems.
4. Because of their digital structure, LSI/VLSI implementation is straight forward.

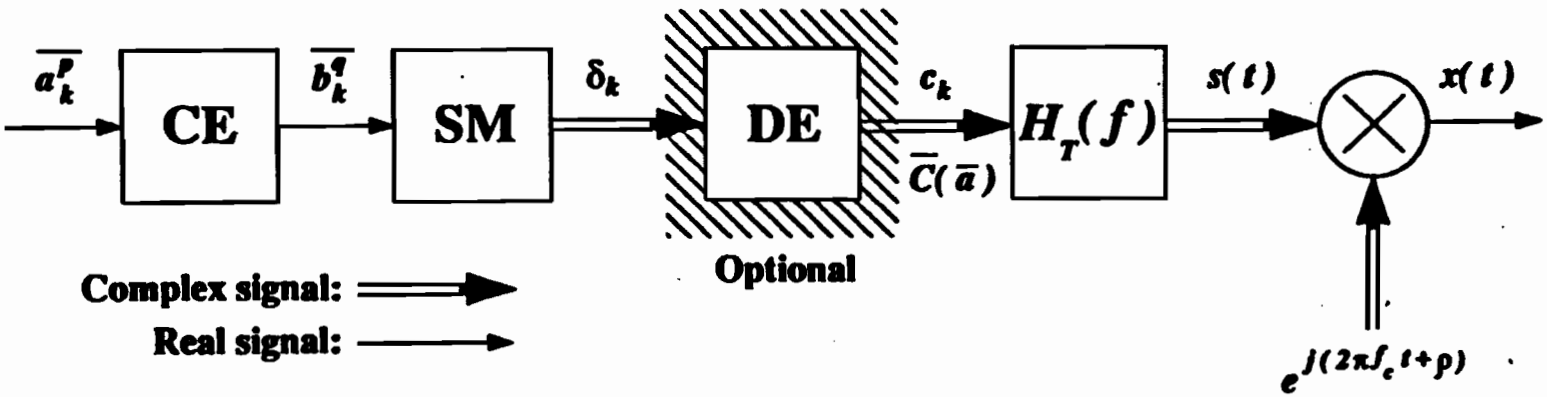

Fig. 1 Block diagram of the transmitter.
CE: Convolutional Encoder
SM: Signal Mapper
DE: Differential Encoder
$H_T(f)$: Transmit Filter

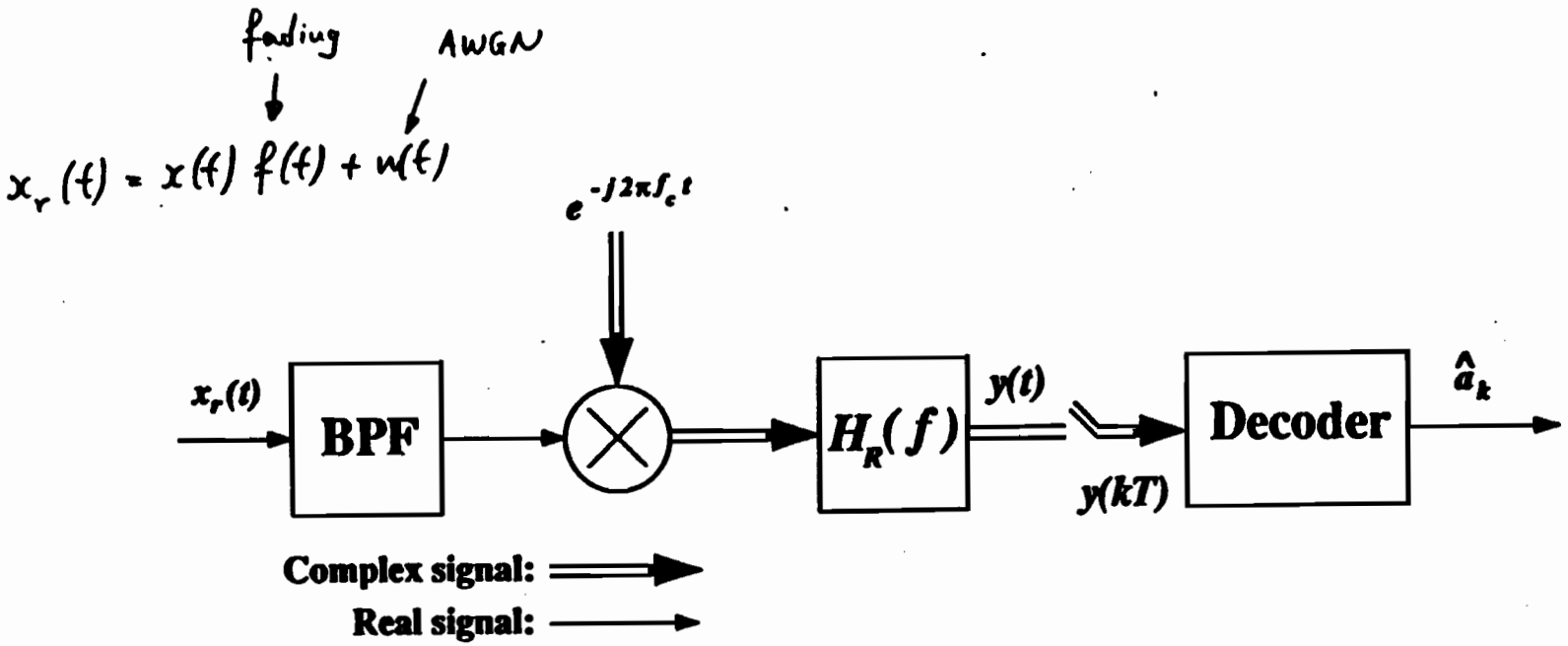

Fig. 3 Block diagram of the receiver.
BPF: Band Pass Filter (roofing)
$H_R(f)$: Receive Filter

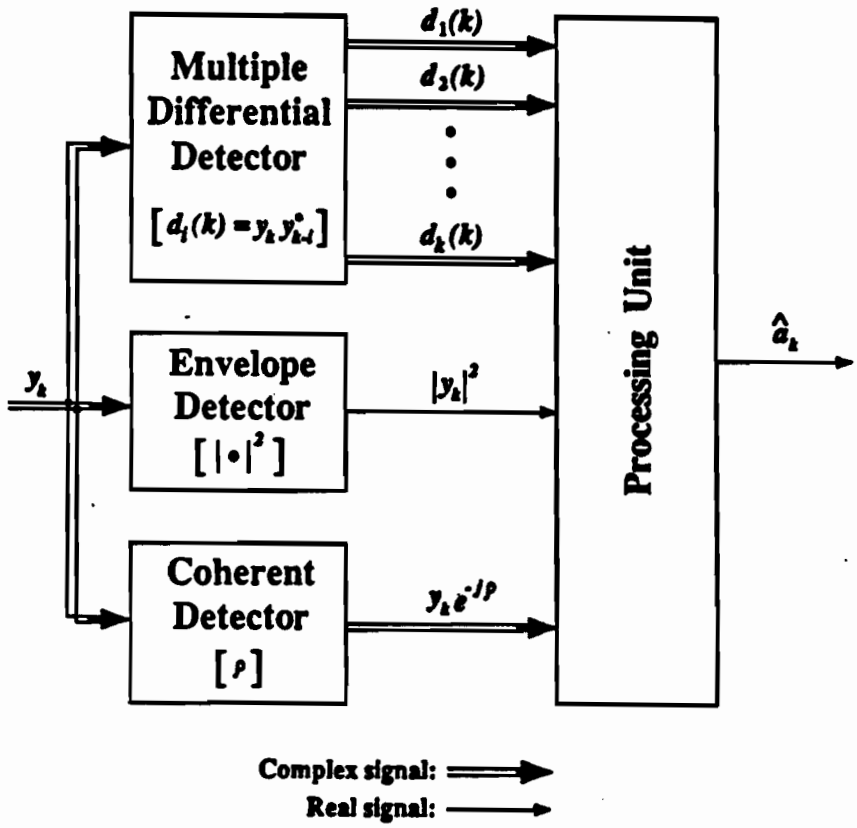

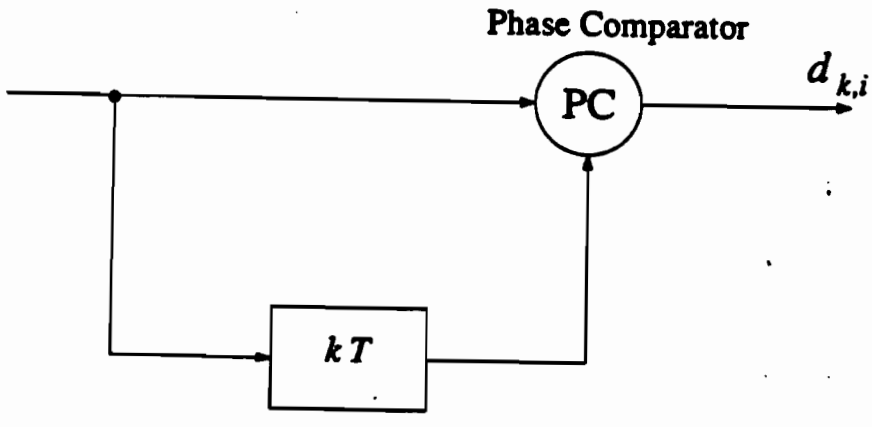

Figure 2 A k-th order differential detector

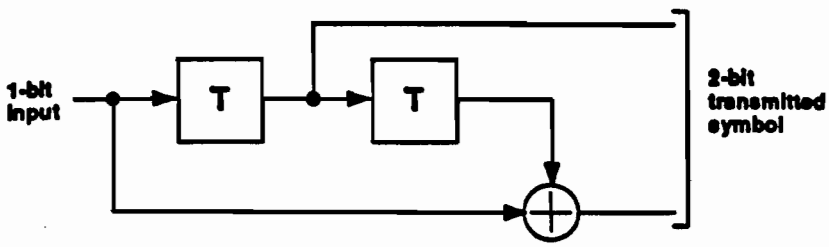

4-state convolutional encoder.

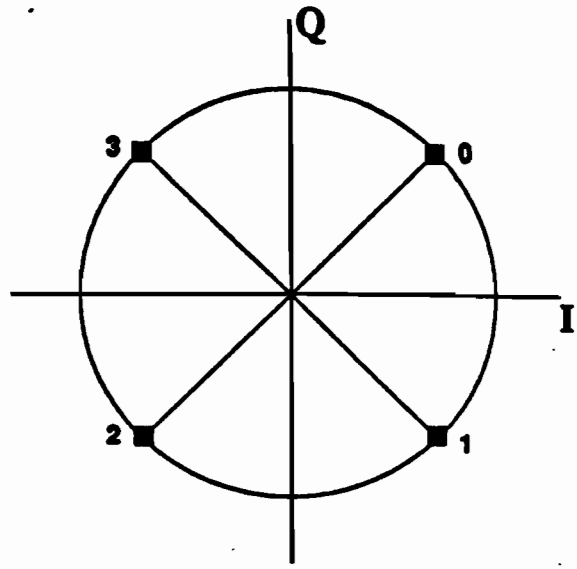

Mapping of transmitted symbols to differential phases.

(a) $\pi/4$-shift DQPSK.

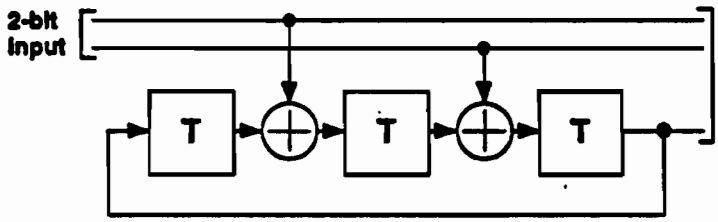

8-state convolutional encoder.

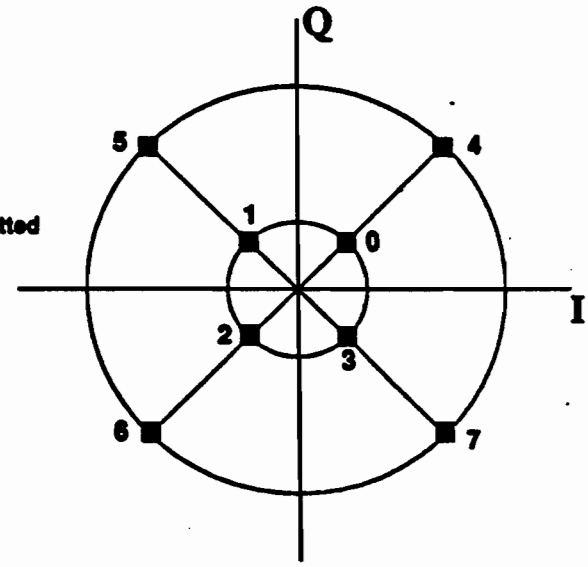

Mapping of transmitted symbols to differential phases & amplitudes.

(b) $\pi/4$-shift 8-DQAM.

Fig. 7 Convolutional encoder structures and signal assignments for the trellis coded schemes under investigation.
(a) $\pi/4$-shift DQPSK
(b) $\pi/4$-shift 8-DQAM

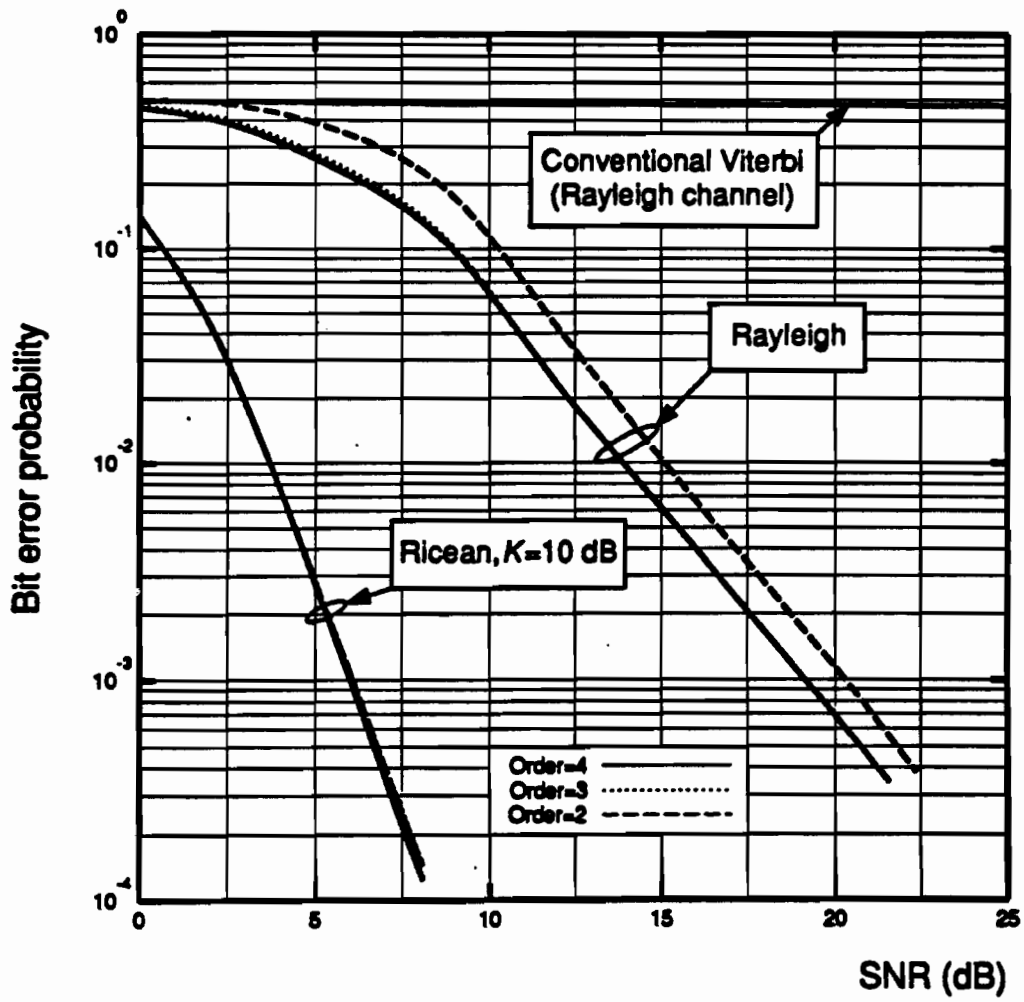

Fig. 9 BER performance of a raised-cosine filtered (α=0.35) rate 1/2 trellis coded QPSK in land-mobile Rayleigh and Ricean (K=10dB) fading channel with B_FT=0.125 employing the new multiple differential receivers with prediction orders z=2, 3 and 4.

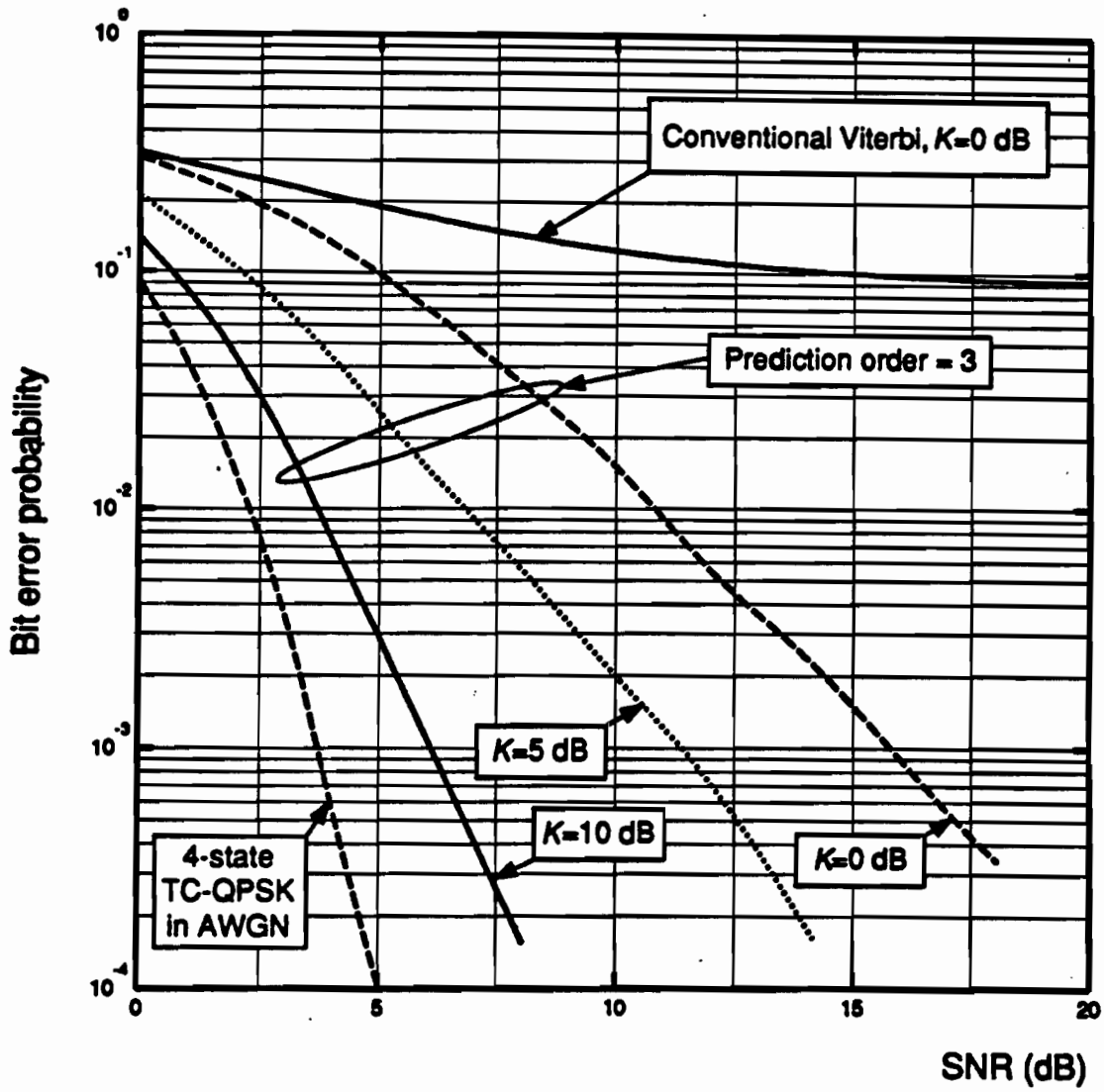

Fig. 10 BER performance of a raised-cosine filtered (α=0.35) rate 1/2 trellis coded QPSK scheme employing the new multiple differential receiver with z=3 in Ricean fading channels.

Fig. 10

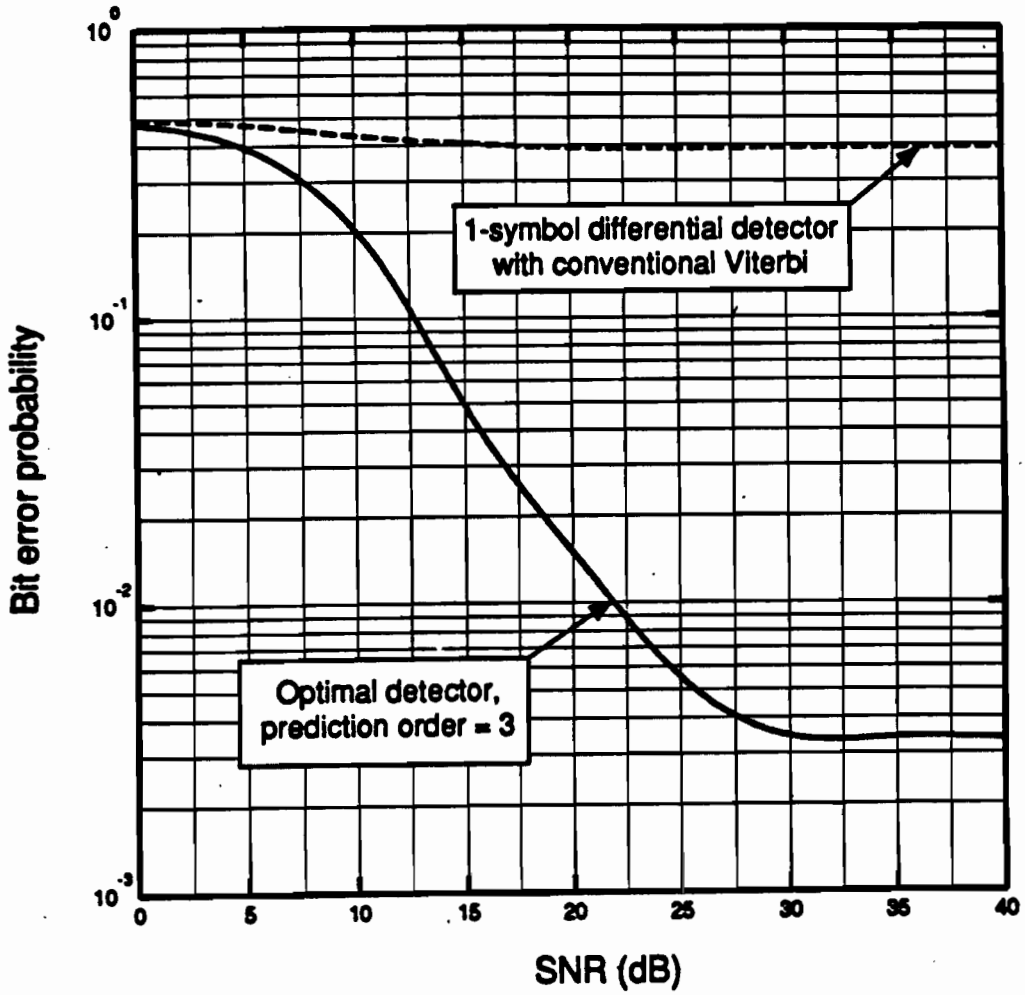

Fig. 12 Comparison of the BER of a 1-symbol differential detector followed by a conventional Viterbi decoder with multiple differential receivers employing z=3 in a Rayleigh land-mobile fading channel having B_FT=0.25.

Fig. 12

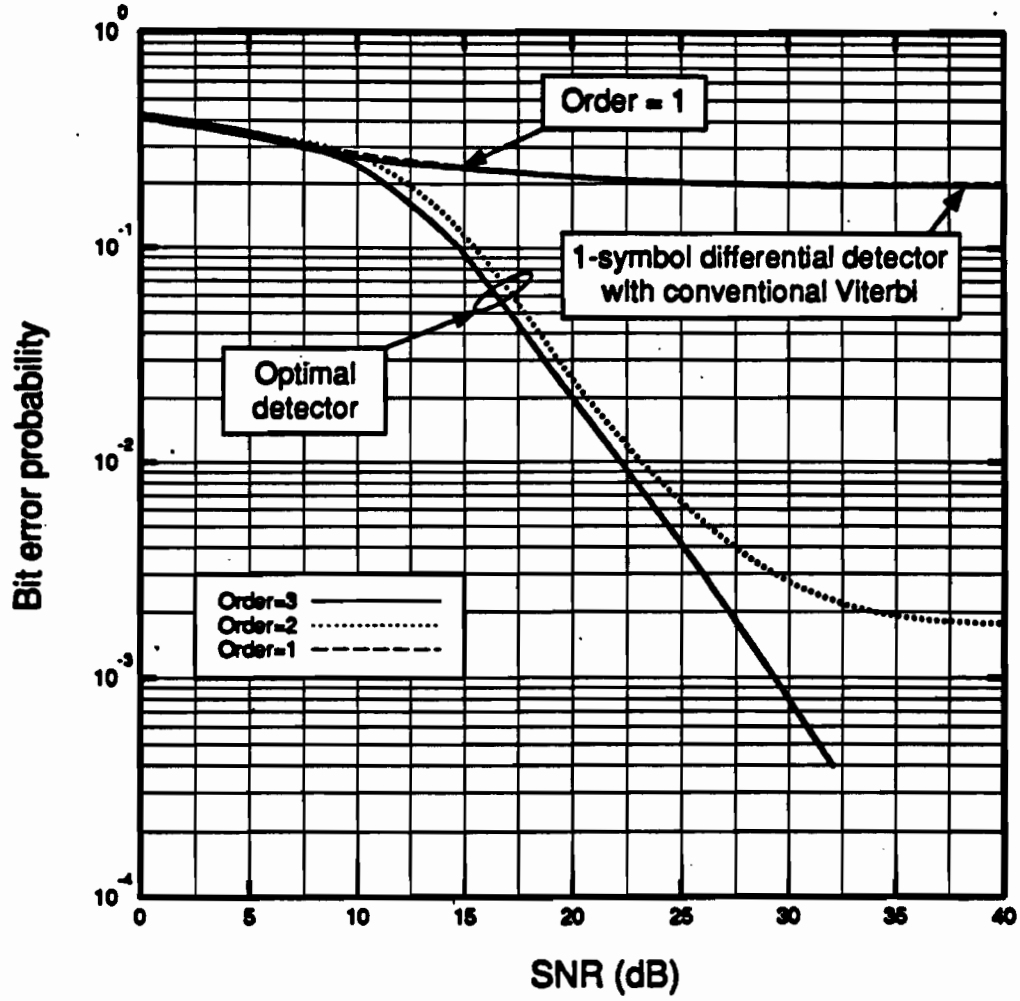

Fig. 13 BER performance of a raised-cosine filtered (α=0.35) rate 2/3 trellis coded 8-DPSK scheme in a land-mobile Rayleigh fading channel with B_FT=0.125 employing the new multiple differential receivers with prediction orders z=1, 2 and 3.

Fig. 13

GMSK — improvements

- Decision Feedback

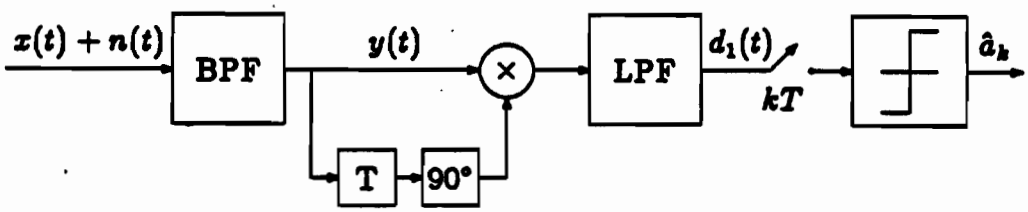

Block diagram of a one-bit differential detector.

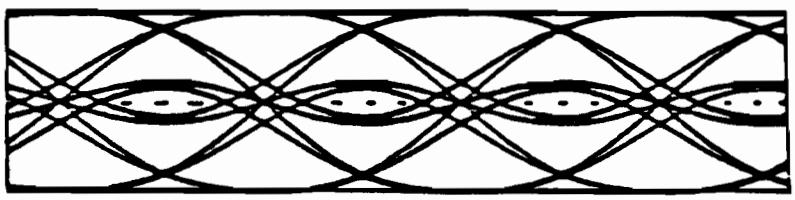

Eye-diagram of a conventional one-bit differential detector.

B_tT	θ_{-3}	θ_{-2}	θ_{-1}	θ_0	θ_1	θ_2	θ_3	$\Delta\theta_{min}$	$\Delta\theta_{min}^{DF}$
0.15	0.3	4.55	21.85	36.6	21.85	4.55	0.3	—	19.6
0.2	—	1.7	20.6	45.4	20.6	1.7	—	1.6	46.2
0.25	—	0.6	18.2	52.4	18.2	0.6	—	29.6	67.2
0.3	—	0.2	15.9	57.8	15.9	0.2	—	51.2	83.4
0.4	—	—	12.5	65.0	12.5	—	—	80.0	105.0
0.5	—	—	10.3	69.4	10.3	—	—	97.6	118.2
1.0	—	—	5.9	78.2	5.9	—	—	132.8	144.6
∞ (MSK)	—	—	—	90.0	—	—	—	180.0	180.0

Phase shifts (in degrees) corresponding to signal, θ_o, and ISI terms (θ_i, for $i \neq 0$) as a function of transmit Gaussian filter B_tT for the one-bit differential detector. $\Delta\theta_{min}$ and $\Delta\theta_{min}^{DF}$ are the minimum differential phase angles before and after applying decision feedback.

Bit Combinations			State	$\Delta\theta_k$
b_{k-1}	b_k	b_{k+1}		(in degrees)
1	1	1	1	88.8
1	1	-1	2	52.4
-1	1	1	2	52.4
-1	1	-1	3	16.0
1	-1	1	4	-16.0
1	-1	-1	5	-52.4
-1	-1	1	5	-52.4
-1	-1	-1	6	-88.8

Differential phase angles $\Delta\theta_k$ of the one-bit detector corresponding to various input data combinations ($B_tT = 0.25$). The contributions of b_{k-2} and b_{k+2} are ignored.

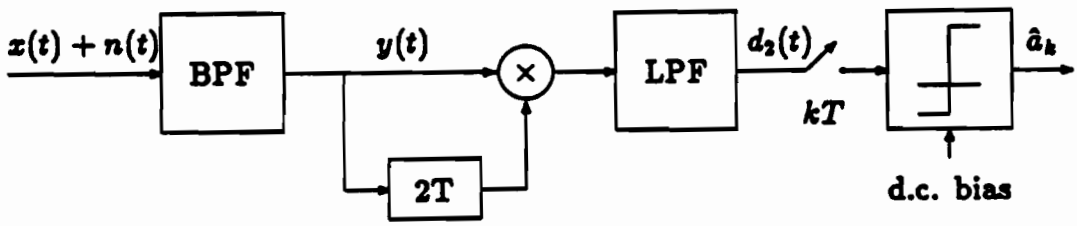

Block diagram of the conventional two-bit differential detector.

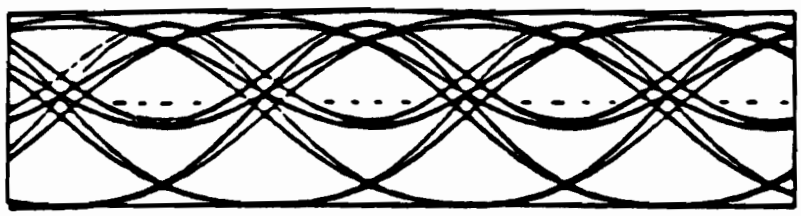

Eye-diagram of a conventional two-bit differential detector ($B_iT = 0.25$).

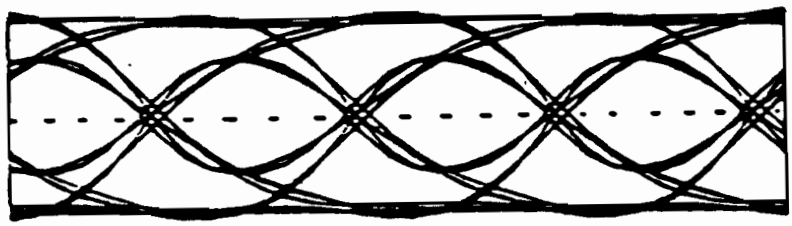

Eye-diagram of one-bit differential detector after applying decision feedback.

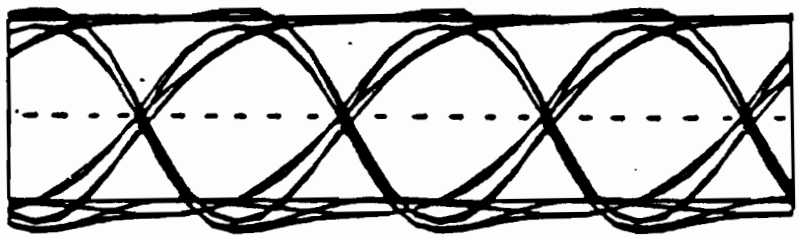

Eye-diagram of two-bit differential detector after applying decision feedback.

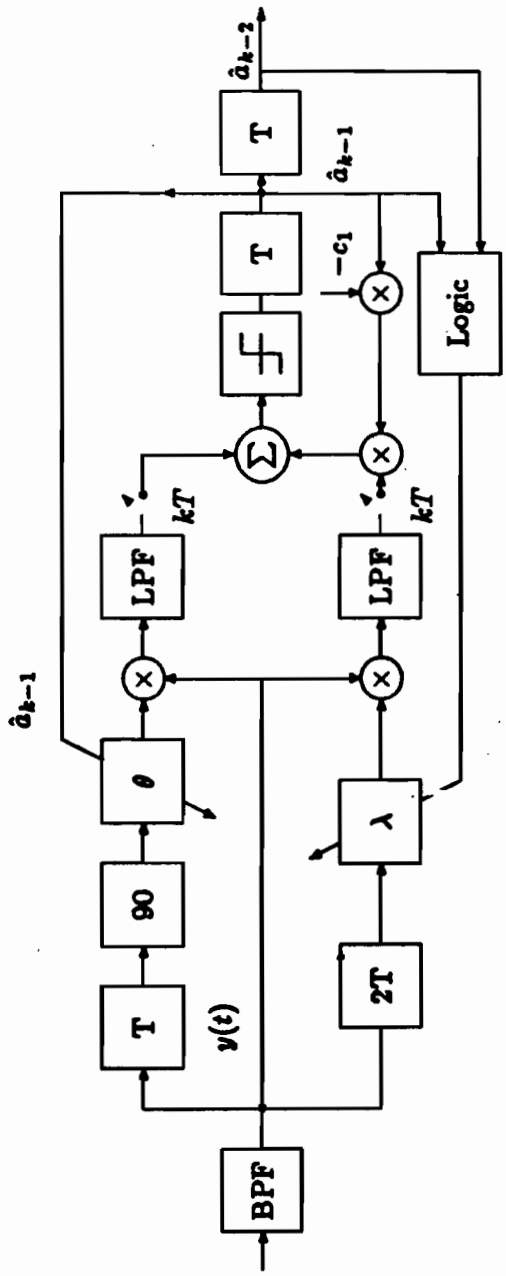

Block diagram of 1+2DF receiver.

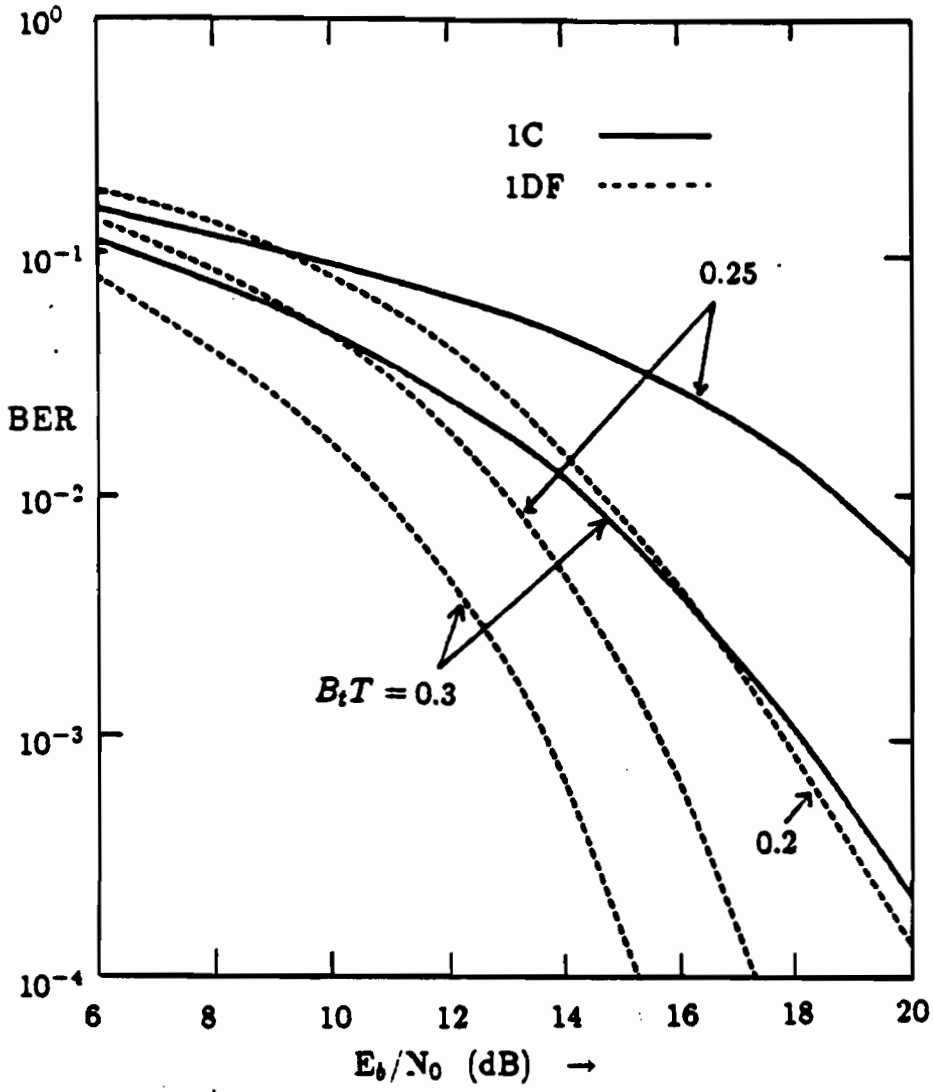

BER performances of one-bit differential detectors (1C: conventional, 1DF: using decision feedback).

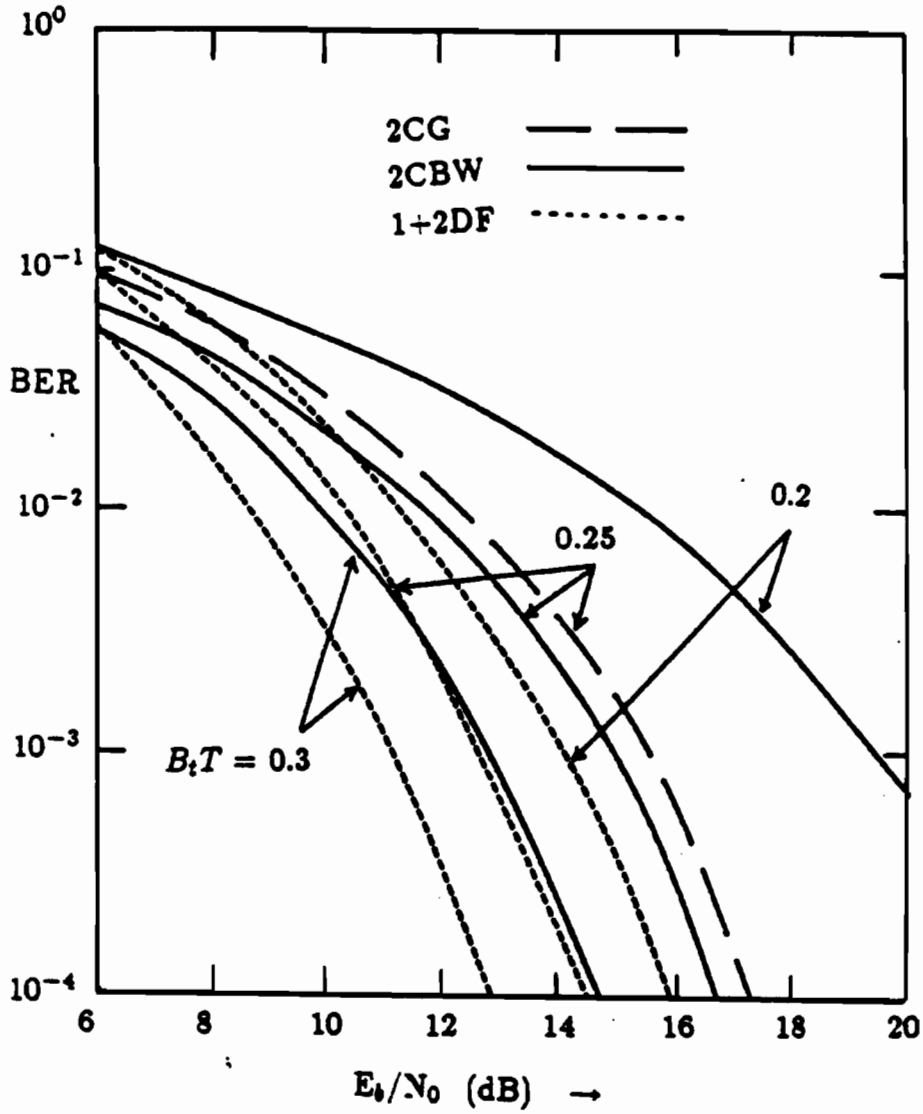

BER performances of conventional two-bit differential detector (2C), and combined one and two-bit differential detectors with decision feedback (1–2DF).

(173)

S. S. Shin & P. T. Mathiopoulos, "Differentially detected GMSK signals in CCI channels for mobile/cellular telecom. systems," in the Proceedings of the Wireless Conf., May 1992

Also: IEEE Trans. Veh. Technology, pp. 289-293, Aug. 1993.

Figure 1 Block diagram of the GMSK transmitter.

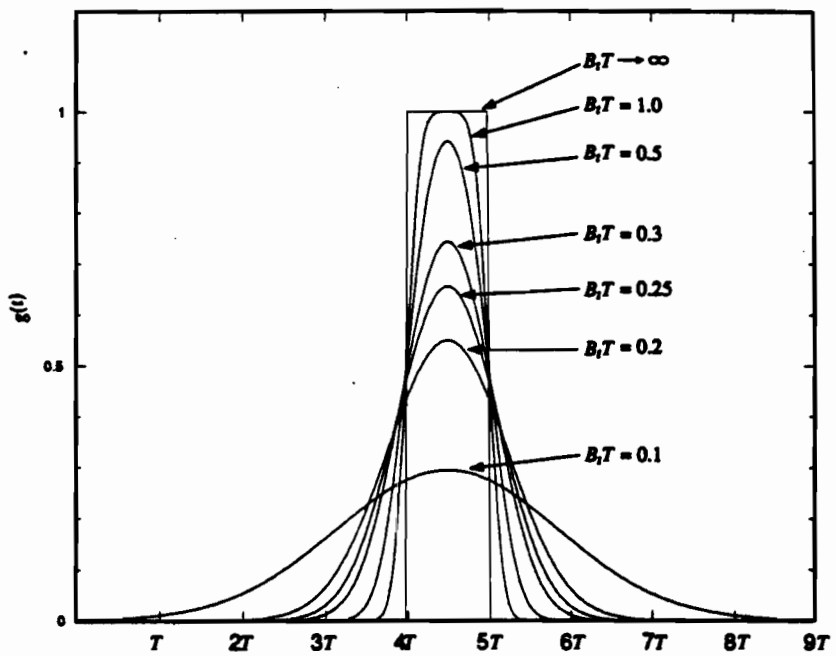

Figure 2 Computer generated graphs of the pulse response $g(t)$ of the Gaussian premodulation filter with B_iT as a parameter.

Table 1 Phases of the signal and the ISI terms (in degrees) for l-bit differential detection of GMSK signal ($B_iT = 0.25$)

l	$\theta_{-2}^{(l)}$	$\theta_{-1}^{(l)}$	$\theta_0^{(l)}$	$\theta_1^{(l)}$	$\theta_2^{(l)}$	$\theta_3^{(l)}$
1	0.6	18.2	52.4	18.2	0.6	—
2	0.6	18.8	70.6	70.6	18.8	0.6

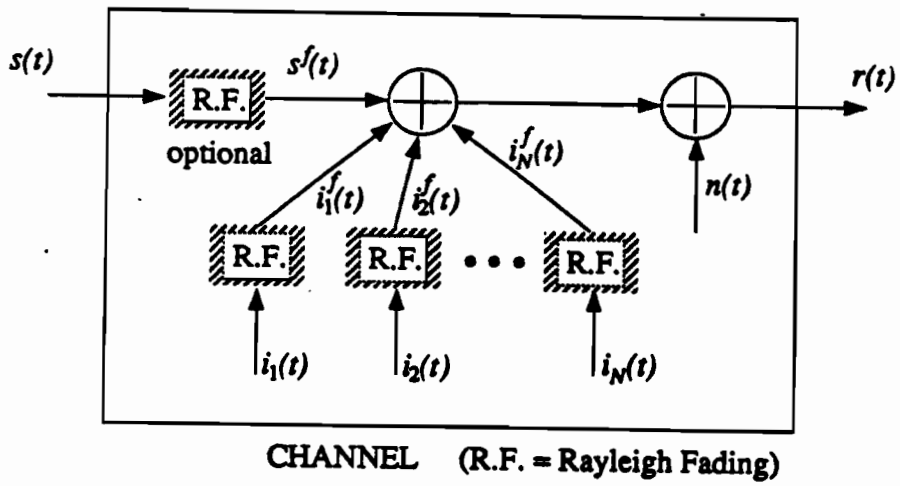

Figure 3 Block diagram of the channel model.

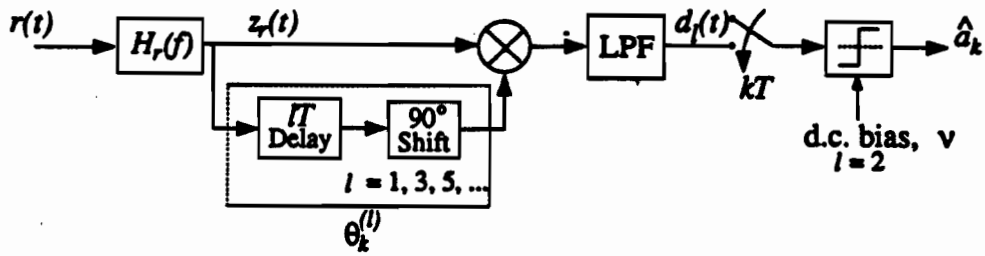

Figure 4 Block diagram of the l-th order differential detector under consideration.

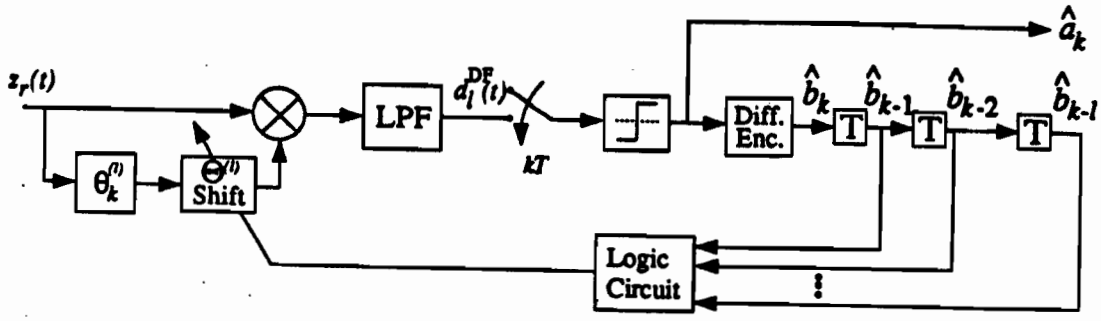

Figure 6 Block diagram of the l-bit differential detection receiver employing the decision feedback (DF) technique.

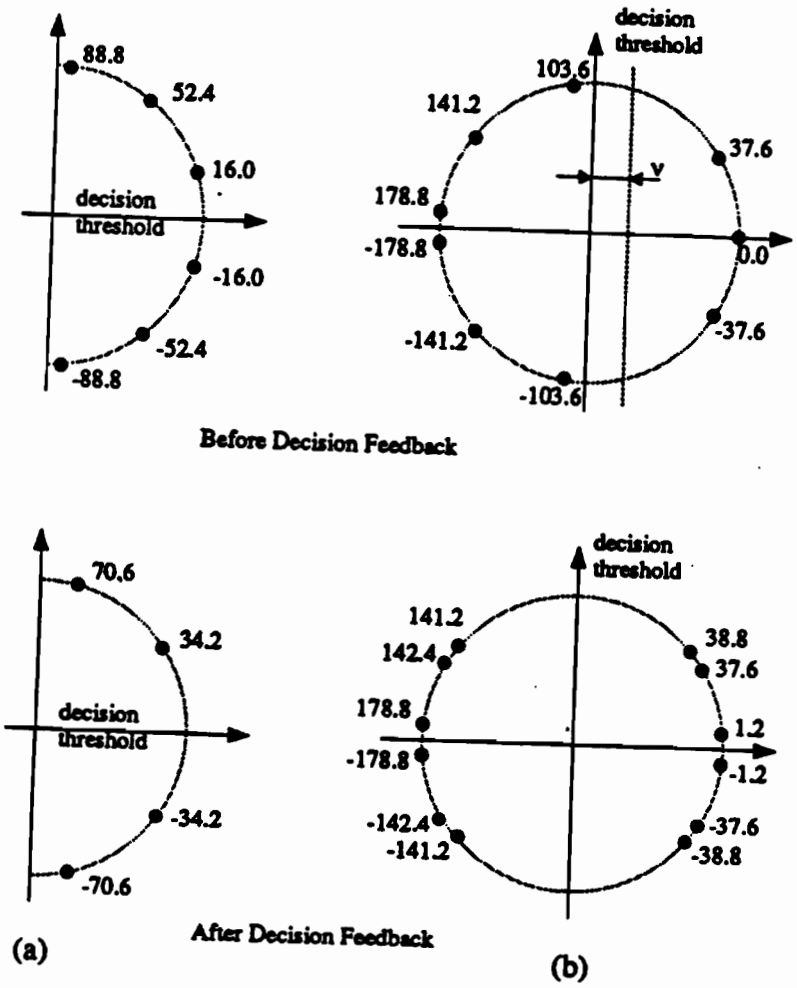

Figure 5 Phase-state diagrams for (a) 1-bit and (b) 2-bit differential detection receiver.

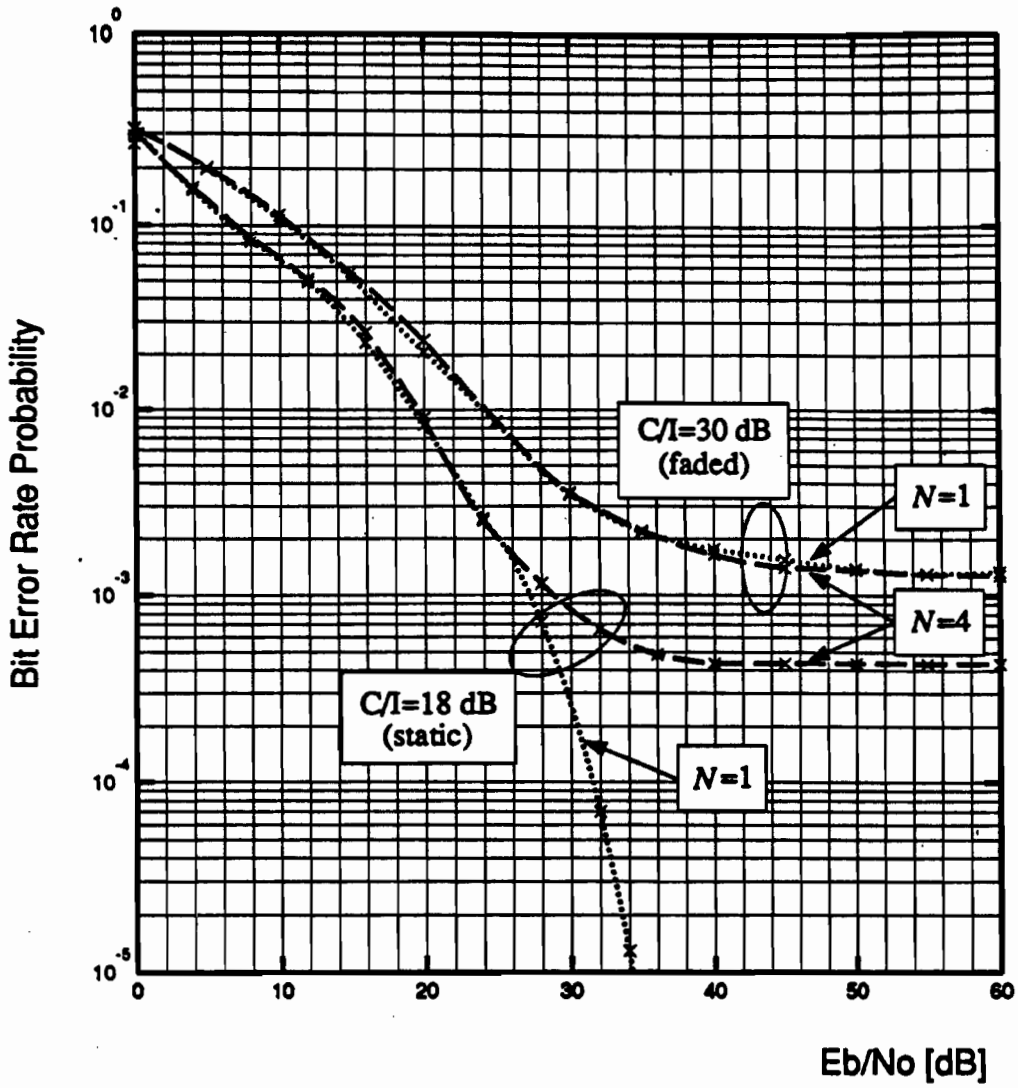

Figure 8 BER performance of conventional 1-bit differentially detected GMSK scheme operated in the presence of static and Rayleigh faded CCI with $N = 1$ and $N = 4$.

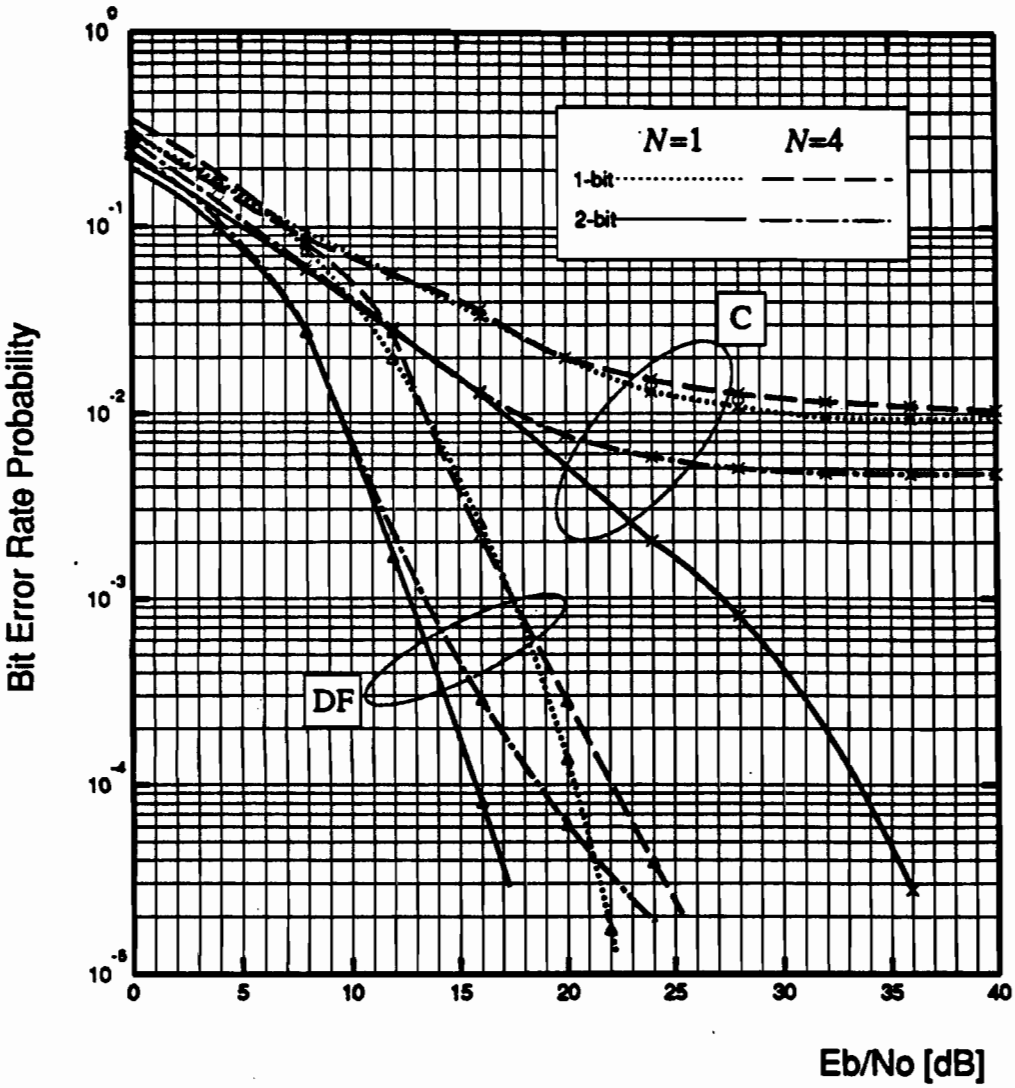

Figure 9 BER performance of the conventional (C) and decision feedback (DF) 1- and 2-bit differential detection receiver in the presence of static CCI (C/I = 14 dB) with $N = 1$ and $N = 4$.

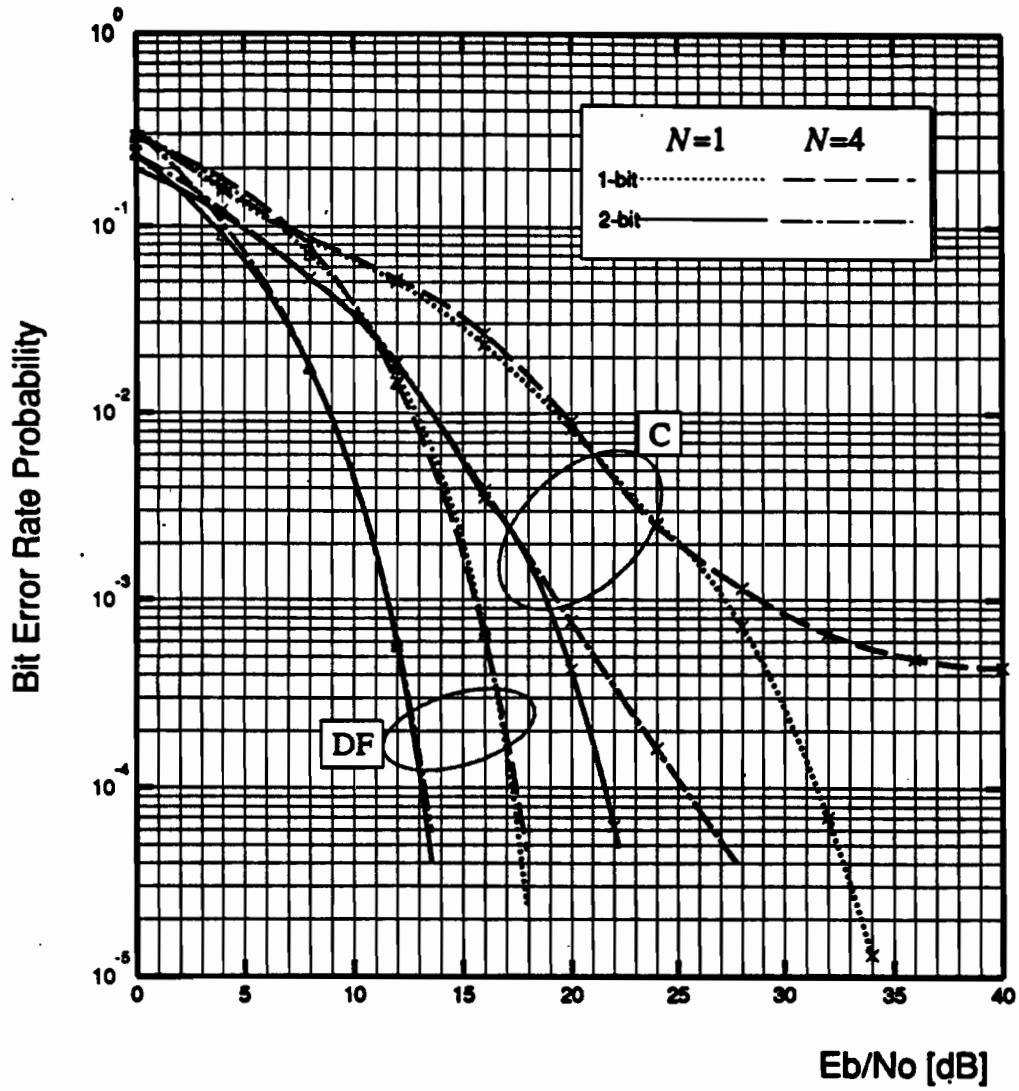

Figure 10 BER performance of the conventional (C) and decision feedback (DF) 1- and 2-bit differential detection receiver in the presence of static CCI (C/I = 18 dB) with $N = 1$ and $N = 4$.

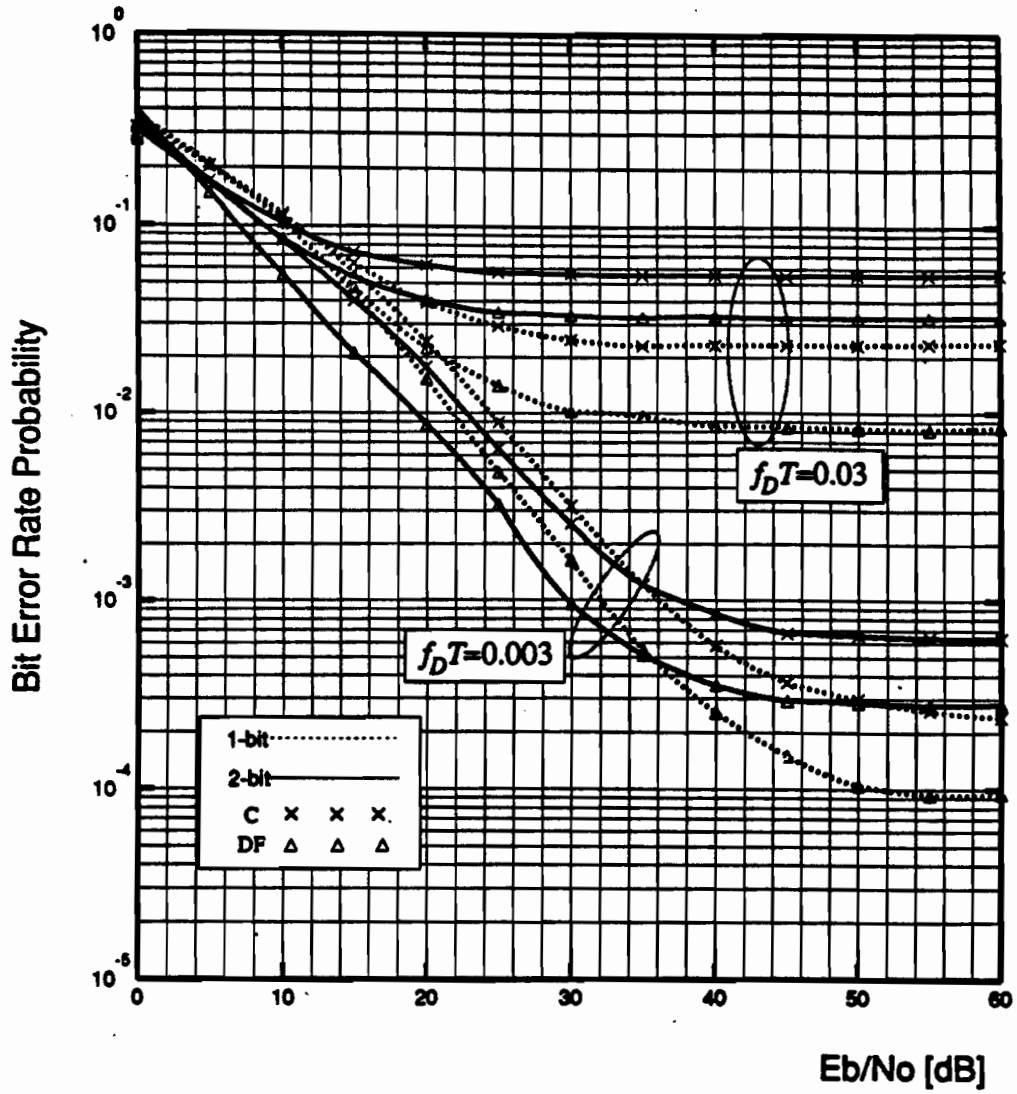

Figure 11 BER performance of the conventional (C) and decision-feedback (DF) 1- and 2-bit differential detection receivers in the presence of fading ($C/I \rightarrow \infty$).

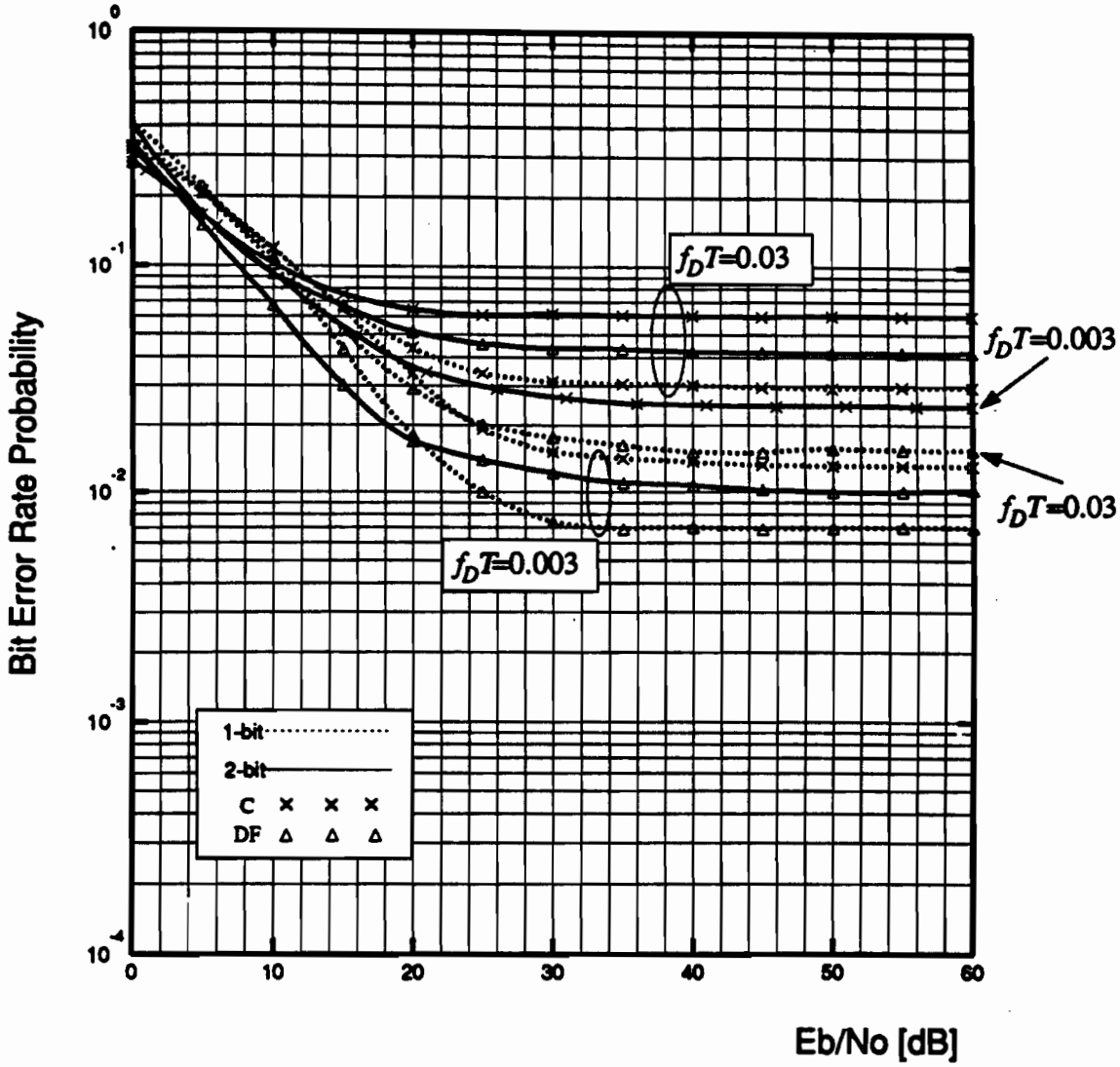

Figure 12 BER performance of the conventional (C) and decision-feedback (DF) 1- and 2-bit differential detection receivers in the presence of faded CCI (C/I = 20 dB).

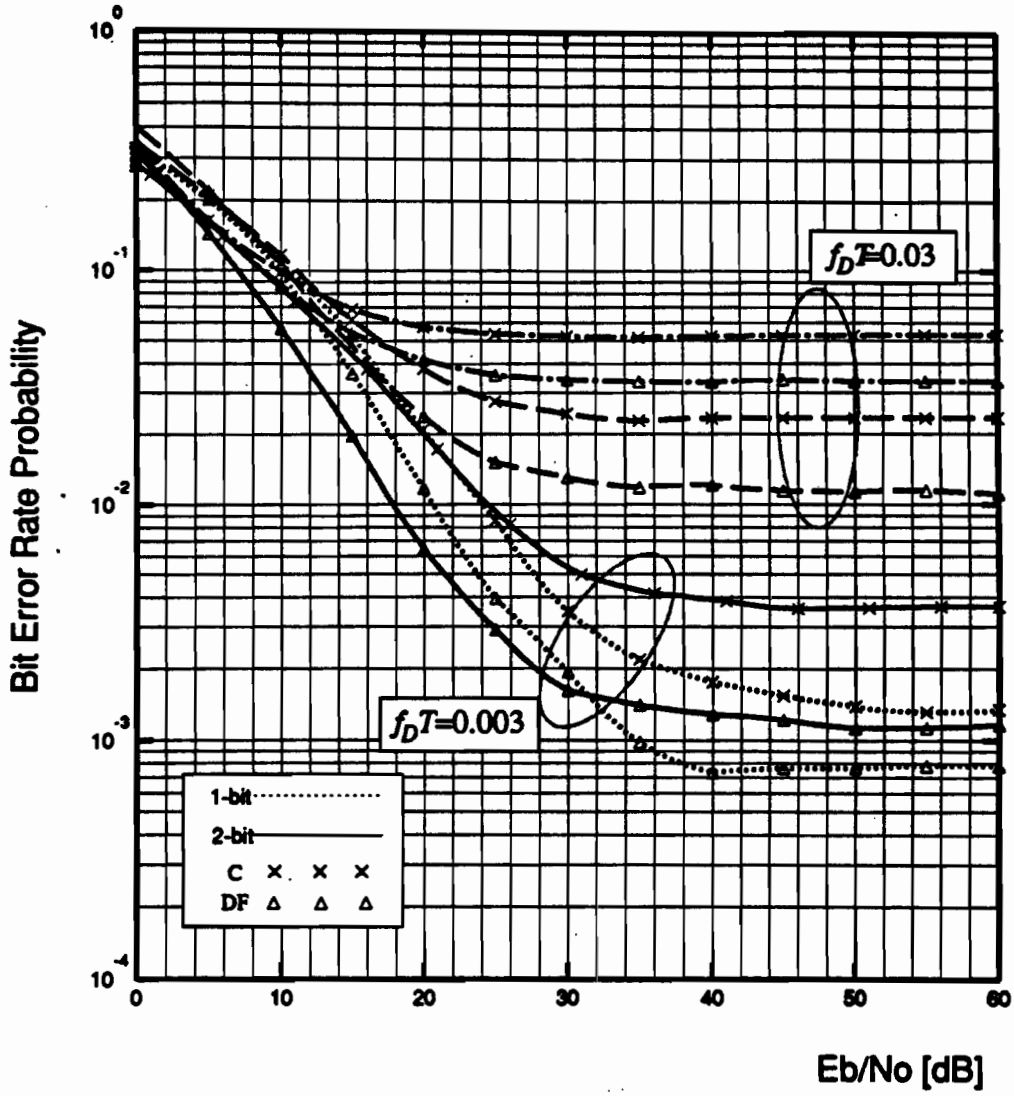

Figure 13 BER performance of the conventional (C) and decision-feedback (DF) 1- and 2-bit differential detection receivers in the presence of faded CCI (C/I = 30 dB).

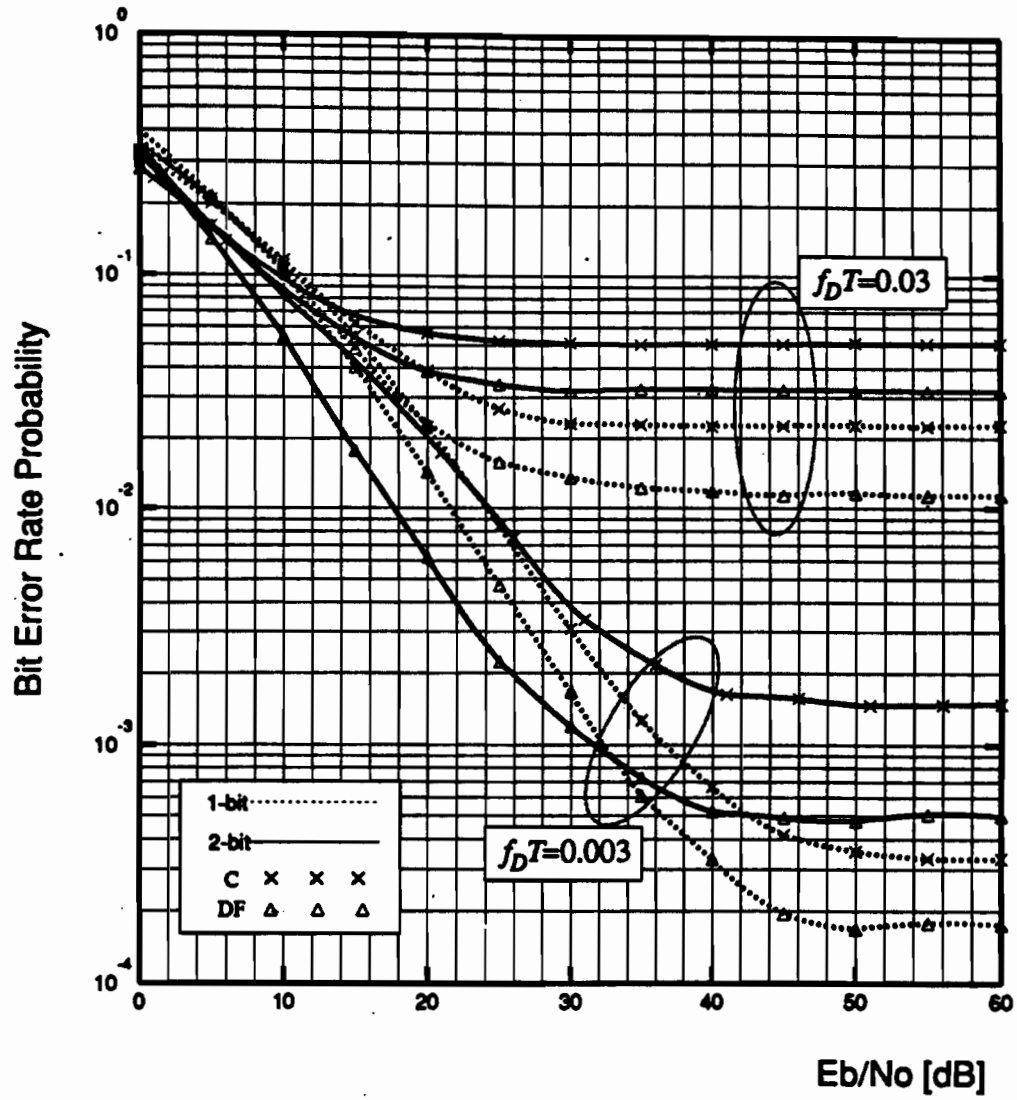

Figure 14 BER performance of the conventional (C) and decision-feedback (DF) 1- and 2-bit differential detection receivers in the presence of faded CCI (C/I = 40 dB).

2 SYSTEM MODEL DESCRIPTION

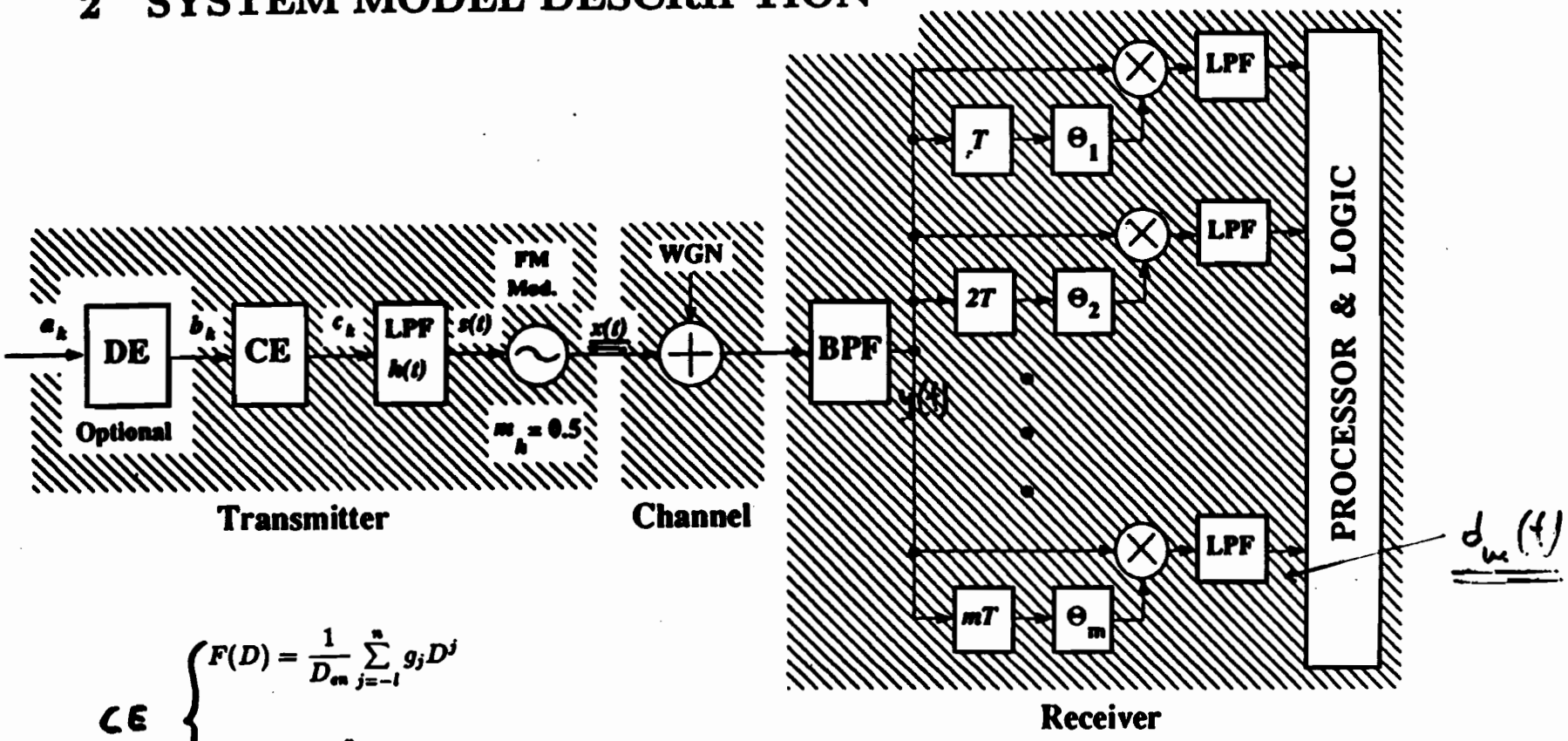

Ref. [R-9] Mahmoud & Mathiopoulos, "Differential detection of CECPM schemes using decision feedback," IEE Proc., Part I, Oct 1991, pp. 473-480.

CE
$$\begin{cases} F(D) = \dfrac{1}{D_{cm}} \sum_{j=-l}^{n} g_j D^j \\ D_{cm} = \sum_{j=-l}^{n} g_j \,. \end{cases}$$

$$c_k = \frac{1}{D_{cm}} \sum_{j=-l}^{n} b_{k-j} g_j \,.$$

$$\int_{kT-T}^{kT} h(\tau)d\tau = \begin{cases} 1 & \text{if } k = 0 \\ 0 & \text{otherwise.} \end{cases}$$ Nyquist I.

$$b(t) = \sum_{k=-\infty}^{\infty} b_k \delta(t - kT)$$

$$s(t) = \sum_{k=-\infty}^{\infty} c_k h(t - kT)$$

$$x(t) = A_0 \cos[\omega_c t + \phi(t) + \psi] \,.$$

$$\phi(t) = 2\pi m_h \int_{-\infty}^{t} s(\tau)d\tau = 2\pi m_h \sum_{j=-\infty}^{\infty} c_j \int_{-\infty}^{t} h(\tau - jT)d\tau$$

$$y(t) = r(t)\cos[\omega_c t + \phi'(t)] + n_{bp}(t)$$

$$d_m(t) = r(t)r(t - mT)\cos[2\pi m_h \sum_{j=-\infty}^{\infty} c_j \int_{t-mT}^{t} h(\tau - jT)d\tau - \theta_m] + n_m(t)$$

$$\theta_m = \begin{cases} 90^\circ & \text{for } m \text{ odd} \\ 0^\circ & \text{for } m \text{ even} \end{cases}$$

$$d_m(kT) = r(kT)r(kT - mT)\cos(\sum_{j=-\infty}^{\infty} c_j V_{k-j}^m) + n_m(kT)$$

$$V_{k-j}^m = 2\pi m_k \int_{kT-mT}^{kT} h(\tau - jT)d\tau \; . \equiv \text{Phase over } mT$$

$$V_k^m = \begin{cases} 1 & \text{for } k > 0 \text{ and } k \le m \\ 0 & \text{otherwise.} \end{cases}$$

$$d_m(kT) = r(kT)r(kT - mT)\cos(\Delta U_k^m - \theta_m) + n_m(kT)$$

$$\Delta U_k^m = \sum_{j=-\infty}^{\infty} b_{k-j} U_j^m \equiv \text{Differential Phase}$$

$$U_j^m = \frac{1}{D_{cn}} \sum_{i=-l}^{n} g_i V_{j-i}^m \; . \equiv \text{Correlative Encoded Phase}$$

For the 1-bit differential detector ($m = 1$)

$$\Delta U_k^1 = \frac{\pi}{2D_{cn}} \sum_{j=-l}^{n} g_j b_{k-j} \; .$$

For the 2-bit differential detector ($m = 2$)

$$\Delta U_k^2 = \frac{\pi}{2D_{cn}} [b_{k-n-1} g_n + \sum_{j=1-l}^{n} b_{k-j}(g_j + g_{j-1}) + b_{k-l} g_{-l}] \; .$$

For the general case where $m \ge 3$ and $n + l + 1 \ge m$

$$\Delta U_k^m = \frac{\pi}{2D_{cn}} \sum_{j=-l}^{m-l} b_{k-j}(\sum_{i}^{l+j} g_{l+i}) + \frac{\pi}{2D_{cn}} \sum_{j=m-l}^{n-1} b_{k-j}(\sum_{i=0}^{m} g_{j-i}) + \frac{\pi}{2D_{cn}} \sum_{j=n}^{n+m} b_{k-j}(\sum_{i=0}^{n+m+l} g_{n-i})$$

For $m > n + l + 1$

$$\Delta U_k^m = \frac{\pi}{2D_{cn}} \sum_{j=-l}^{n-1} b_{k-j}(\sum_{i=0}^{l+j} g_{-l+i}) + \frac{\pi}{2} \sum_{j=n}^{m-l} b_{k-j} + \frac{\pi}{2D_{cn}} \sum_{j=m-l}^{n+m} b_{k-j}(\sum_{i=0}^{n+m+l} g_{n-i}) \; .$$